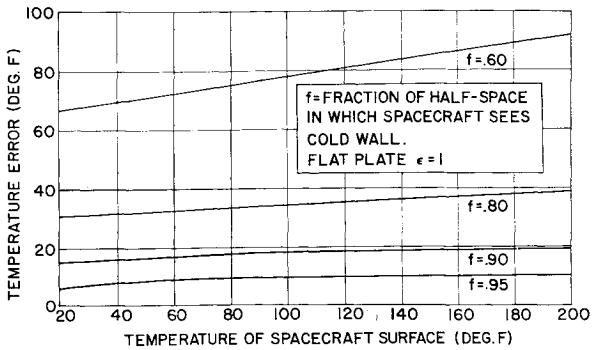

Fig. 2 Infrared reflection errors from solar simulator optics.

from the spacecraft will be returned to the cryogenic wall of the chamber and not the test object. In such a system the spacecraft will see by reflection only cryogenic wall in the collimators, thus achieving the effect of a continuous cryogenic wall about the test volume.

Some magnitudes of reflection errors from thermal energy emitted by a test object are shown in Fig. 2, where f is the fraction of half-space in which a point on the spacecraft sees the cold wall directly or by reflection off the collimating mirrors. The quantity $(1 - f)$ is a measure of half-space in which the spacecraft sees some part of itself by reflection.

Emission errors are the result of the thermal radiation emitted from the solar simulator optical elements. This error can be reduced by cooling the optics to low temperatures where the emitted energy is small, or by maintaining a low emittance coating on the surface of these elements. Either method is suitable for reducing the emitted energy to a level near that which would be expected from the cryogenic wall; however, cooling the optics may result in the distortion of these elements and may cause vapors in the chamber to condense on them, which would degrade their reflective characteristics during a test.

The reflective coating on collimating elements is usually aluminum, although the emissivity of aluminum (about 0.03 in the infrared) is not sufficiently low to reduce the thermal radiation from the collimators at ambient temperature to that of a liquid nitrogen cryogenic wall. However, the resulting thermal error for a spacecraft, at near ambient temperatures, will be very small even if the collimators occupy as much as one-third of a hemisphere of the space environment chamber.

Radar Video Data Handling

THOMAS J. BURKE*
Radio Corporation of America, Moorestown, N. J.

FOR years the exclusive function of the monopulse radar has been to acquire and track a single target, with emphasis on the radar spherical coordinate data, AGC, servo errors, and alignment errors for obtaining precise post flight trajectory measurements. Until recently, little attention has been given to monopulse radar data which gives information on all targets illuminated in the radar beam—the video information, which consists of the detected i.f. data from the radar receivers. The tracked target data is gated and used in the range and angle tracking loops to maintain automatic lock-on,

Presented as Preprint 63081-63 at the AIAA Space Flight Testing Conference, Cocoa Beach, Fla., March 18–20, 1963; revision received October 15, 1963.

* Leader, Data Handling Systems.

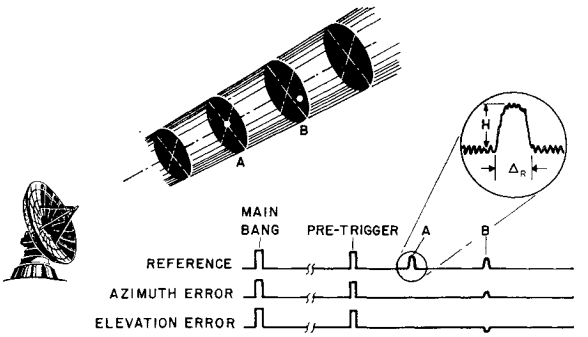

Fig. 1 Radar video.

and the ungated video provides information on untracked targets. The main bang or transmit pulse is emitted by the radar and the return echoes are received by the same antenna.

In Fig. 1, target A is the tracked target and target B is another target offset from the radar line of sight. The video from the azimuth and the elevation error receivers yield pulses which provide a measure of the offset of B, which can be accurately determined (through calibrations), and the amplitude (H) of the B target can be corrected to a value equivalent to that for a tracked target. Pretrigger pulses are precisely located relative to the A target, and the B target moves relative to them.

The transverse video record/playback system described below was made possible by developments in the TV industry. Subsequent advancements have been helical scan (continuous) recording, which eliminates the need for video multiplexing, and high-speed longitudinal recorders with up to 15 tracks for use with a multiple radar installation. The processing and reduction methods for such improved systems would be identical to those described here.

Video Recording

Video data are recorded by equipment (Fig. 2) which closely resembles standard TV studio recorders. The general TV requirements of frequency response (4 Mc) and signal/noise ratio (36 db) closely satisfy the requirements of radar video recording. However, the timing stability must be improved to give short- and long-term stabilities of approximately 10^{-5}. The radar return signals are processed in the microwave section, from which the azimuth and elevation signals are mixed with the local oscillator, and 30-Mc i.f. outputs are available to the receivers.

The reference signal represents the total energy received by the radar, and the azimuth and elevation error signals represent the difference between the target positions in their planes. The phase relations between the i.f. reference and error signals determine the directions of deviation, and the relative amplitudes between the i.f. reference and error signals determine the deviations. These three channels are fed to the wide dynamic range (WDR) receivers, which provide linear logarithmic amplification (without gating or gain control), which is maximum on weak signals and minimum on strong signals.

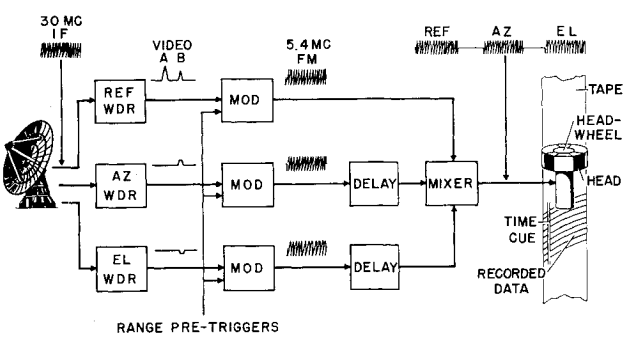

Fig. 2. Radar video recording.

The video output (detected from the amplified i.f.) has a dynamic range of 32 db compressed from an 80-db input. Range pretrigger pulses, inserted into each channel and modulated and mixed into a single channel for recording, provide control to a time-division multiplex section, to allow recording of range segments of reference data and of the error channels in sequential order. The pretriggers are selected so that the ungated video that is recorded is nominally balanced around the tracked target, e.g., in a 285-prf case, 50,000 yd in and 100,000 yd out in range relative to the tracked target. A headwheel, which makes one rev/prf, has three heads (120° apart) which sweep in order transversely across a tape with a head-to-tape speed of 1800 ips, yielding high band width and high utilization of tape. Each head records one channel of data; one revolution creates three transverse tracks of data, with reference, azimuth, and elevation, in that order. Tone wheel control, real time, and audio commentary are also recorded on low-bandwidth tracks.

The radar and recording system is thoroughly calibrated, usually by both pre-mission and post-mission signal strength calibrations on a boresight tower and radar tracking of a sphere of known cross section lofted by a balloon. With a transmitted pulse of 1 μsec duration, a small target will produce an echo of 1 μsec duration. For a long target, such as the wake of an entry vehicle, the echo can be elongated to 10 μsec.

Video Playback

When recorded video data are played back, and the reference video is displayed on an oscilloscope, the display appears just as it did to the A scope operator during the mission, except that the true fluctuations of the pulses appear, because there is no AGC action. To determine which off-axis targets and which time spans are of interest, photographs are taken of the oscilloscope display. The playback unit is similar to the recorder, except that it has only the playback capability.

The FM data channels of reference, azimuth, and elevation are read out in segments. The pretriggers extracted from the tape provide sync for delay sweeping of a scope and generation of a tracking gate similar to A scope displays for the radar operator. A gate controls a video switch for passing the three channels of selected target video through sample and hold circuits and A/D converters. A range counter measures the range from the pretrigger to the gated target video. Since the true range of the pretrigger is available via other recording media, the total range of the gated target will be available after subsequent processing. The digital equipment then accepts the real time (to 0.01 sec), range, reference, azimuth, and elevation data, as well as identification, parity, and sync bits for transfer to the digital tape recorder at the standard 200 character/in. packing density, for reading into a 709 computer at 75 ips.

Figure 3 illustrates the flow process for reducing the calibrations. A calibration curve of signal/noise ratio vs amplitude

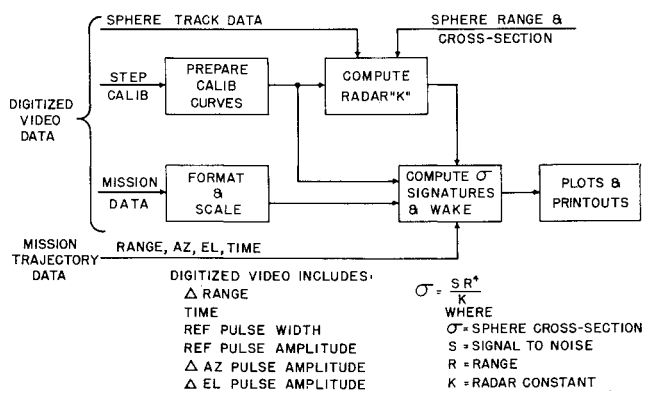

Fig. 3. Video processing flow.

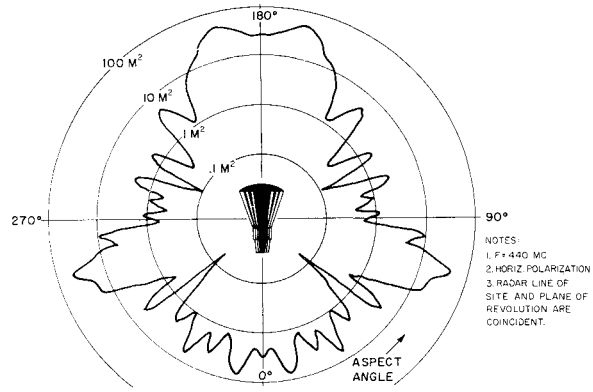

Fig. 4 Mercury capsule back-scatter characteristics.

is obtained. A radar constant K is then computed using the known sphere cross section, sphere range, and the derived signal/noise ratio. The digitized mission data are time-correlated with the mission trajectory data (processed from other recorded media) to obtain true target range and true off-axis azimuth and elevation. The reference signal amplitude is corrected to an equivalent on-axis value. The corrected reference digital quantities are then converted to signal/noise numbers by the calibration curve, and K is used to obtain the pulse-to-pulse cross section of the target.

The cross section of the tracked target can be determined by the pulse-by-pulse processing (it has no azimuth or elevation off-set corrections) and compared with AGC cross-section data. The latter does not, however, contain the bandwidth of the video cross section (AGC is derived from a low-pass audio-range filter). Hence the sharp variations of cross section due to slight attitude changes, which the video data observe in each pulse, are not often detected in the AGC data. This is a vital factor when precise off-axis target signature data are to be obtained for which there are no AGC data.

Identification of shape and space attitude of a target is a great problem. Many complex objects have been identified, but only by a trial and error process using known signatures for cones, cylinders, spheres, and flat plates, which are applied in a computer program to come up with an estimate of the size and shape of the unknown target. For a known target in the tracking radar beam, such as the Mercury capsule (Fig. 4), for which anechoic chamber measurements have been made on scaled models, the processed cross-section data can be examined for specular reflections and lobing patterns to identify the capsule and determine its attitude. However, this can only be done from extra-atmospheric radar video data; when the capsule enters the atmosphere, a shock front develops, causing ionization and a long wake, which is frequency selective. The effect is dependent on the density and thickness of the ionized media, as well as on the incident angle of the electromagnetic waves; the wake reflects the radar frequency and hence destroys the signature measurement capability. Since the wake is reflective, causing an elongation on the return pulse, wake length can then be determined by the equation shown in Fig. 5, where the transmit pulse width Δ_T and the frequency of light C are known, and the echo pulse width Δ_R and the angle between the velocity and range vectors can be found from video and trajectory data. Wake measurements have been made at C-band, L-band, uhf frequencies, and the theories of electron density having reflection and absorption effects are borne out. C-band wake lengths have been measured to be over 2000 ft and measured L and uhf wakes have been proportionately greater on the same target.

Concluding Remarks

Video pulse-by-pulse processing can now be done by a fully automated system, with data repeatability within 1 db. One

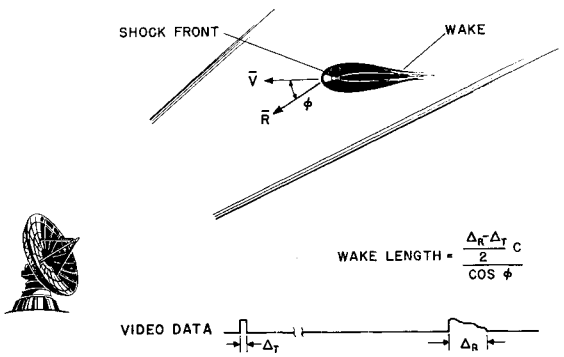

Fig. 5 Radar video during re-entry for measurement of wake length.

application of real (or near-real) time radar video processing might be an osbital attitude sensing system, which would provide a means for evaluating the accuracy of the spacecraft's self-contained guidance and attitude sensors. Other possible applications include an orbiting vehicle identification system and penetration-aid study programs. Results obtained from wake analysis will aid re-entry studies relating to communication blackout, since radar returns are also similarly affected by the ionization.

Design of Cylinder-Cone Intersections

HERBERT BECKER*
Allied Research Associates, Concord, Mass.

The basic theory for stresses at coaxial intersections of uniform thickness cones and cylinders has been developed. In the procedure to be described below, the structural and geometric requirements are revealed for a uniform stress intersection. However, an intersection fabricated to meet these requirements would be impractical. An arbitrary simplification has been made to obtain a low stress ("optimum") intersection of a more practical character. The principal features of this intersection are the absence of stress concentration and the ability to withstand internal forces without exceeding a stress level equal to the cylinder circumferential membrane stress.

Nomenclature

C = stress ratio, $\sigma t_0/pR$
D = bending rigidity of shell, $Et^3/[12(1-\nu^2)]$, in-lb
E = Young's modulus, lb/in.^{2}
M = bending moment per inch of circumference, lb
p = pressure, lb/in.^{2}
Q_0 = transverse shear per inch of circumference at intersection, lb/in.
R = mean radius of cylinder, in.
t = thickness of shell, in.
t_0 = thickness of cylinder away from intersection, in.
t_1 = thickness of intersection at springing line, in.
α = cone semiangle
λ = attenuation length of cylinder, $\{R^2t^2/[3(1-\nu^2)]\}^{1/4}$
ν = Poisson's ratio
σ = stress, psi

Presented as Preprint 2892-63 at the AIAA Launch and Space Vehicle Shell Structures Conference, Palm Springs, Calif., April 1–3, 1963; revision received October 17, 1963. This investigation was performed under contract to the U. S. Navy Department Bureau of Ships. The writer wishes to express his appreciation to John Vasta of that department for permission to publish the results.

* Director, Engineering Sciences. Member AIAA.

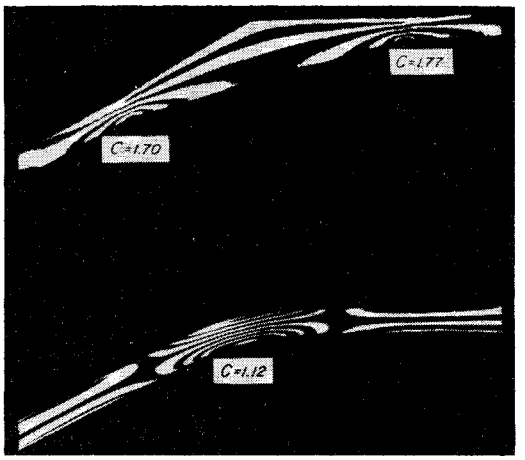

Fig. 1 Stress ratios for two types of intersections.

Design Procedure

AN investigation of stresses at cone-cylinder intersections with various types of reinforcement rings revealed that the simpler designs were accompanied by lower stress fields. It was also found that the character of the stress field in an axial cross section could be reproduced in a two-dimensional model of the cross section loaded by the internal forces that were computed using standard three-dimensional (or axisymmetric) shell theory. Therefore, the design procedure discussed herein is based upon the two-dimensional analysis of a beam-like strip of the cone-cylinder axial cross section loaded by the internal forces at the intersection of the cone-cylinder pressure vessel subjected to internal pressure.

Examination of mathematical data[1] and photoelastic studies[2, 3] revealed striking symmetry of the stress distribution about the interior angle bisector of the cone-cylinder intersection. This is depicted in Fig. 1 by the fringe patterns on two models. The first has a low stress level at the intersection springing line but has concentrations at the tangent points, whereas the second is essentially free of tangent concentrations but is overstressed at the springing line. This symmetrical stress distribution suggested that for design purposes the interior forces at the intersection of a cylinder with a cone of half-angle α could be replaced by those for an intersection consisting of two cones each of half-angle $\alpha/2$, as shown in Fig. 2. The problem was simplified further by as-

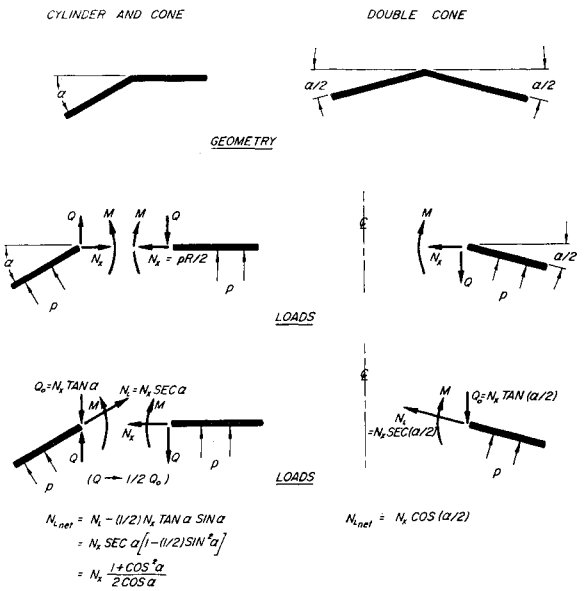

Fig. 2 Geometries and forces at equivalent cylinder-cone intersections.